In Situ Laser-Induced Fluorescence and Ex Situ Cavity Ring-Down Spectroscopy Applied to NO Measurement in Flames: Microprobe Perturbation and Absolute Quantification

Nathalie Lamoureux, Pascale Desgroux

In-situ LIF and ex-situ CRDS applied to NO measurement in flames: microprobe perturbation and absolute quantification

Nathalie Lamoureux, Pascale Desgroux

Univ. Lille, CNRS, UMR 8522 - PC2A - Physicochimie des Processus de Combustion et de l'Atmosphère, F-59000 Lille, France

Special Issue in Memory of Prof Mário Costa

Keywords: microprobe, gas sampling, NO, LIF, CRDS

Supporting Information: Supplementary Materiel show the pictures of the microprobes, a side view of the experimental setup and the measurements of the gas flow rate in the probe.

Abstract:

Flame-sampling experiments allow describing the species profiles in function of the height above the burner. Even with microprobes as those generally used for Gas Chromatography measurements, the perturbations induced by the microprobe can be non-negligible. Not only the heat losses due to its presence will affect the temperature and the spatial position of the species profiles, but the composition of gas sampling may be altered. In order to attempt to clarify the induced-perturbations by microprobes, NO species profiles are obtained in stoichiometric low-pressure flames using either in-situ LIF or ex-situ absorption measurements. Gas samplings are performed with two uncooled-quartz microprobes characterized by their tip angle (6.6° and 16°), and analyzed in an external absorption cell by CRDS (Cavity Ring-Down Spectroscopy). The absolute quantification of the NO mole fractions is undertaken in the burned gas using either the standard addition method by LIF (Laser Induced Fluorescence) or after gas sampling from the integrated spectral absorptivity by CRDS. In the burned gas, it turns out that the gas sampling is altered by the microprobe having the smallest tip angle where the absolute mole fraction of NO is found 40% lower than when the quantification is performed either after gas sampling with the largest tip angle microprobe or by in-situ LIF. As expected, the comparison of the relative NO profiles along the flame indicates that the profiles measured after gas sampling are shifted downstream. This is all the more so as the tip angle is large and the flame clearly attached. Kinetic simulations based on the probe geometry and the residence time does not allow us to discern possible homogeneous or heterogeneous reactions inside the probe. The most disturbing factor is attributed to a cooling effect due to the probe.

1 Introduction

Gas sampling and subsequent analyses are necessary for measuring the chemical composition of the reactive mixture in combustion processes. One of the important factors to consider in obtaining accurate measurements is the design of the probe.. For instance, probes have been specially designed with a supersonic expansion and helium dilution for sampling the gas of aircraft engines exhaust [1] or with a specific orifice design in a 30 kW laboratory scale furnace [2]. Stainless water-cooled probes are also used for probing the gas sample in small scale combustors, for example in Costa's group for studying mild combustion [3] and flameless combustion [4]. Species profiles are currently measured after sampling gases in laboratory scale burners either by Molecular-Beam Mass Spectrometry (MBMS) through cone probes or macroprobes, or by Gas Chromatography (GC) or MS through microprobes.

Since the development of the MBMS techniques, the probe disturbance due to the cone has been the purpose of a large number of papers [5–15] and review-papers [16–19]. The pioneering study of Biordi et al. [5] characterized the probe perturbation on the species profiles along the flame axis of the major stable species measured by MBMS using different cone probes (orifice size, cone angle). The effect on the temperature was measured by a thermocouple located beneath the orifice of the tip. The cooling effect near the tip was shown, and it was estimated that a 100 K correction could reasonably be applied at the highest flame temperature. It was shown that the species profiles measured with a conical probe were shifted towards the burned gas compared to a species profile measured with a microprobe such as those used with GC analysis. The extensive literature [5–19] has made it possible to characterize the cone-disturbance with the geometric size of the cone, the tip opening, the residence time of the sample in the cone,…, with respect to temperature and species perturbations. Depending on the size of the orifice and the angle of the cone tip, the species profiles may be affected not only in their shape but

also in their absolute mole fraction values. With the advantage offered by the MBMS technique to measure radical species in burner-stabilized flames, OH or CN species have been measured by using Laser-Induced Fluorescence (LIF) beneath the cone tip, and compared to the MBMS results [6–8,20] or measurements of OH by Electron Spin Resonance (ESR) [21]. It is shown that the presence of the probe generates a shift downstream of the species gradient, and a decrease of the radical species density in the preheated zone of the flame. Regarding the absolute concentration of the species in the burned gas, the literature reports that it is sometimes unchanged [6,20] or changed [7,21]. The explanation for these observations may be due to the cone geometry or to the distance 1/ between the tip and the burner, and 2/ between the tip of the cone and the laser axis[8,21]. As shown in Refs. [7,8], the diffusion of OH or CN is blocked by the nozzle in the reactive zone, but not further in the burned gas.

Modeling calculations have been performed to simulate the probe-induced perturbation in burner-stabilized flames [9–11], indicating that smaller cone angles disturb the flame less spatially but more the composition of the gas sample. 2-D and 3-D modeling including CFD (Computational Fluid Dynamics) or DNS (Direct Numerical Simulation) simulations have been performed to analyze the probe-induced effects [12,13]. The presence of the cone induces violations of the one-dimensionality of the flame. These simulations highlight that the heat losses, the disturbance of the temperature field and of the species streamlines around the tip depend on the distance between the tip and the burner surface. Subsequently, the location of the gas sample below the tip is affected. Interestingly, Gururajan et al. [13] determined that the supporting flange of the probe has also a notable effect on the flame structure that becomes two-dimensional. The temperature perturbation remains the most important one. For instance, in a burner-stabilized stagnation flame, Saggesse et al. [22] took advantage of the plate to perform soot sampling through a device embedded into the stagnation plate. The comparison between 1-D and 2-D computational results and experimental measurements indicates that the flow

through the central orifice can introduce notable effect on the temperature close to the plate and on the soot size distribution. A complete temperature map can be measured by using Kr X-Ray fluorescence in low-pressure flames [14,15]. Results show indeed a strong disturbance of the temperature around the cone tip, and the temperature correction may be as high as several hundreds of Kelvins. Thus, Hansen and co-workers [14,15] recommend to simulate the flame structure with a two-dimensional code in order to consider the radial perturbations induced by a cone probe.

Microprobes are routinely used to probe gas samples in stationary flames or in Jet Stirred Reactors (JSR) for further analysis of the stable species by GC for example. Such microprobes are recognized to generate limited disturbance of the temperature profiles [23]. Contrary to the "sonic" probe as used in MBMS, the gas sample probed with a microprobe is transported in a molecular flow. As mentioned by Heitor and Moreira [24], the sampling flow rate and the size of the suction orifice are set as a compromise between the required low pressure to achieve aerodynamic quenching of chemical reactions and the minimum flow rate for the chemical analyzers. Kramlich and Malte [25] have modeled the pressure and temperature variations inside the microprobe by considering one-dimensional gas flow conditions. They have simulated the conversion of NO into NO_2 inside the tip taking into account reactions which can occur at the probe-wall and in the gas phase. The results are in a good agreement with the experimental measurements of NO and NO_2 performed after gas probe sampling in a JSR apparatus. Colket et al. [26] have developed a gas-dynamic model to describe the gas flow and the heat transfer inside the probe. They conclude that an aerodynamic quenching is unlikely to occur in microprobes, but chemical quenching rates may be sufficient to freeze reactions.

In an atmospheric flat-flame seeded with NO, Zabielski et al. [27] have compared the NO concentration measured in the burned gases either by in-situ optical absorption or after gas sampling

through a cooled quartz microprobe as designed by Colket et al. [26] by using a chemiluminescence analyzer. Within the experimental data precision (±10%), no major discrepancies related to processes occurring in the probes are identified. Li et al. [28] have measured NO in the burned gas region of flames seeded with NH_3 either by Laser Saturated Fluorescence calibrated by the NO addition method or by a chemiluminescence analyzer after gas sampling through an uncooled quartz probe with a 1 mm diameter orifice. They have observed a discrepancy of 5-7% of the NO amounts between the two techniques. They mention the possible conversion of NO into NO_2 in the probe due to the recombination reactions that occur in the presence of O-atoms as proposed by Allen [29]. Schoenung and Hanson [30] have compared the absolute mole fractions of CO measured in the burned gas either in-situ by laser absorption or after gas sampling through microprobes (uncooled quartz or cooled stainless steel) by a non-dispersive infrared analyzer. Based on these measurements, they have indirectly observed some conversion of CO into CO_2. They have analyzed the difference of the absolute mole fractions from the chemical equilibrium predictions of CO/CO_2, and from the aerodynamic model proposed by Colket et al. [26]. In addition, results obtained with an uncooled quartz probe or a water-cooled stainless steel probe show some discrepancies, especially in the lean flame conditions and with the increase of the probe sampling pressure. They recommend to work at a reduced pressure downstream of the probe (around 50 mbar). Kaiser et al. [31] have analyzed the effect of the residence time in an uncooled quartz microprobe on the species concentrations. The measurements of stable species (hydrocarbons, CO, CO_2, …) have been performed using GC at different HAB in an atmospheric C_3H_8/air flame. From these measurements, they concluded that close to the burner surface some pyrolysis and oxidation reactions occur in the microprobe. These reactions are limited by decreasing the residence time, i.e. decreasing the sampling pressure. In the reaction

zone, the reactions are reduced due to the lowest concentration of hydrocarbon species, and the perturbation of the species profiles is attributed to the "attachment" of the flame to the probe.

Besides, gases may also be probed through a fused silica capillary tube as undertaken in counterflow diffusion flames [32–34]. Despite the very small size of the capillary tube, its introduction also generates disturbance as identified using non-intrusive measurements like particle image velocity (PIV) [33] or Planar LIF [32,33].

Although microprobes can be intrusive, they have been widely used to measure stable species profiles in different types of flames [35–41]. The question of the disturbance of the microprobe for the analysis of the flame structure often arises during the chemical modeling of the flame. Indeed, the kinetic modeling calculations are frequently performed with the introduction of a temperature profile. This profile is either determined by thermocouples or by non-intrusive laser techniques. It turns out that the temperature profiles can be adjusted and shifted towards the burned gases so that the position of the simulated species profiles matches that of the experimental profiles obtained after microprobe sampling [35,37,38]. On the contrary, this shift requirement is canceled out when the simulation is compared with the species profiles measured in-situ as done previously [42]. It therefore turns out that until now the disturbance of the probe is manually compensated because of the lack of knowledge concerning the intrusiveness of the microprobe in the flame. It is the objective of our work to help clarify this disturbance.

To do this, the present work aims to compare in-situ and ex-situ measurements of NO in low-pressure neat $CH_4/O_2/N_2$ stoichiometric flat flames (p = 5.3 kPa and 10.6 kPa). In these flames, the NO is formed through the prompt-NO pathway. Therefore, its profile presents a gradient in the

reactive zone followed by a plateau in the burned gas with few tenth of ppm. NO species is chosen because its kinetic formation is very sensitive to temperature. It is measurable either in-situ by LIF or after gas probe sampling using CRDS. This absorption laser-based technique is highly sensitive [43–45]. It has been used by Evertsen et al. [46] to measure the absolute NO mole fraction in a diesel engine exhaust. Two methods of calibration are used, one based on the NO standard addition method (SAM), the other relying on a direct quantification by absorption. Temperature profiles are measured by in-situ NO-LIF thermometry.

In this work, we analyze the microprobe disturbance both on the shape of the NO profile (position and gradient) and quantitatively (amount of NO measured with and without the microprobe). To assess our approach two different designs of microprobe are investigated together with two different pressures. This last parameter allows to act on the proximity of the species gradient with respect to the burner. Finally, an analysis based on kinetic calculations of the reactions inside the probe and in the flames is conducted in order to identify the perturbations introduced by the probe on the temperature.

2 Experimental setup

2.1 Low pressure burner and gas supply

Experiments have been undertaken in stoichiometric laminar $CH_4/O_2/N_2$ premixed flames stabilized above a 6-cm diameter bronze water-cooled McKenna burner (Holthuis & Associates). Volumetric flow rates of the gas mixture are regulated by using Mass Flow Controller (MFC) at 0.48/0.96/3.35 slpm (in standard (273.15 K, 1.013×10^5 Pa) L/min) for $CH_4/O_2/N_2$ respectively. An additional line with a low range MFC (0.1 slpm) is connected to the premixed gases inlet of the burner to seed the mixture with known amounts of NO (for the standard addition method) from a commercial preparation of 2001 ppmv NO diluted in N_2 (standard S1 with ± 2% precision). Two flames, named flame F1 and

F2, have been studied at p = 5.33 and p = 10.66 kPa (40 and 80 Torr), respectively. Flame F1 is identical to the one previously studied in our team [42]. Details concerning the burner and gas supply are given in[42,47]. The temperature profile of the flame was obtained in-situ by NO-LIF thermometry (without microprobe). In the present work, the temperature profile in flame F2 is measured following our recent work [48,49], while the previous measurements are used in the flame F1 [42]. The temperature determination is described in Section 2.3.1 and the profiles are presented in Section 4.2.

The burner enclosure is equipped with different optical accesses allowing in-situ laser diagnostics (LIF). The laser beam passes through the central axis of the optical ports located 13 cm below the top flange of the vessel. This flange is equipped with a port for the microprobes. Microprobe is installed at a fixed position such as its tip is approximately 13 cm below the flange. The burner is movable in the vertical direction. A side view of the burner is given in the Supplementary materials (Figure S2). For the in-situ measurements, the height above the burner (HAB) is defined by the distance between the laser axis and the burner surface. For the probe sampling measurements, the HAB is defined by the distance measured between the microprobe tip and the burner surface with a cathetometer. Profile measurements in function of HAB are performed from the burned gases to the burner surface. The probe is withdrawn during all in-situ measurements.

2.2 Probe sampling and absorption cell

Gas sampling is performed through different uncooled quartz microprobes in order to perform the ex-situ measurements of NO by using CRDS in an external absorption cell. Two shapes of microprobe are examined. The tip is designed with a cone drawn out to a cylindrical tube (section 1) as shown in Figure 1~~Figure 1~~. This first section is extended with a cylindrical tube (section 2) identical for both microprobes (inner diameter equal to 9.8 mm). The tip microprobes are opened with a 200 µm diameter orifice. The first microprobe (microprobe P1) is very sharp with an inner cone half-angle

about 3.3° over 23 mm length, and an area ratio of 255. The second one (microprobe P2) has an inner cone half-angle about 7.9° over 14.7 mm length, and an area ratio of 750. Note that the area ratio represents the ratio of the surface area between the bottom of the cone and the tip opening. The thickness of the cylindrical tube is 0.6 mm. The length of the cylindrical section is equal to 27 mm (36 mm) with an inner diameter equal to 2.85 mm (4.3 mm) for the microprobe P1 (and P2). The total volume of the tip and the first section is equal to 0.2 and 0.6 cm^3 for the microprobe P1 and P2, respectively. They are also characterised with a surface/volume ratio (*S*/*V* ratio) equal to 35.1 cm^{-1} and 23.2 cm^{-1}, respectively. All the geometric characteristics are summarized in **Table 1**.

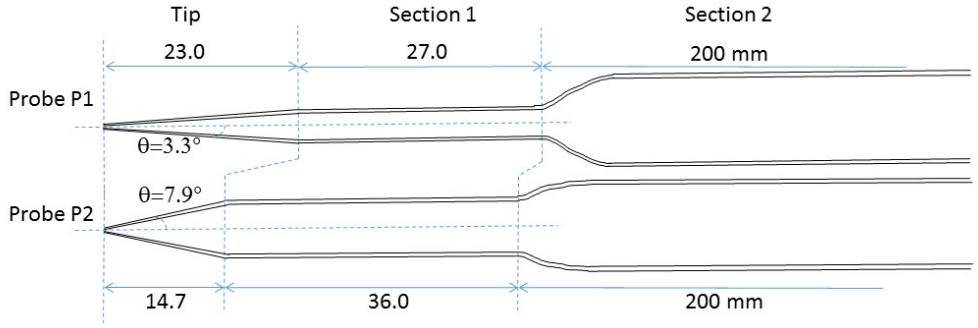

Figure 1. Microprobes drawings (top: P1, bottom: P2).

Table 1. Geometric characteristics of the microprobes P1 and P2.

Probe	Tip			Section 1			Tip + section 1	
	half-angle θ (°)	length (mm)	Area ratio	Inner diameter (mm)	Length (mm)	Residence time (ms)	volume (mm^3)	*S*/*V* ratio (mm^{-1})
P1	3.3	23	255	2.85	27	1.3	200	3.51
P2	7.9	14.7	750	4.3	36	3	600	2.32

The stainless steel absorption cell, with a 3 cm inner diameter, measures 39.5 cm long. Gases are injected through a Teflon tube either from the probe gas sampling or from a commercial preparation of 10.6 ppmv NO diluted in N_2 (standard S2 with ± 5% precision) as shown in Figure 2~~Figure 2~~. In order to prevent the adsorption/desorption phenomena at the wall, gases in the cell are in continuous flowing. The pressure was stabilized at the desired value (controlled with a 0-100 Torr pressure gauge) by using an automatic regulating valve (Leybold, CMOVE1250). The gas temperature was controlled by a thermocouple (type K) at the inner wall of the cell.

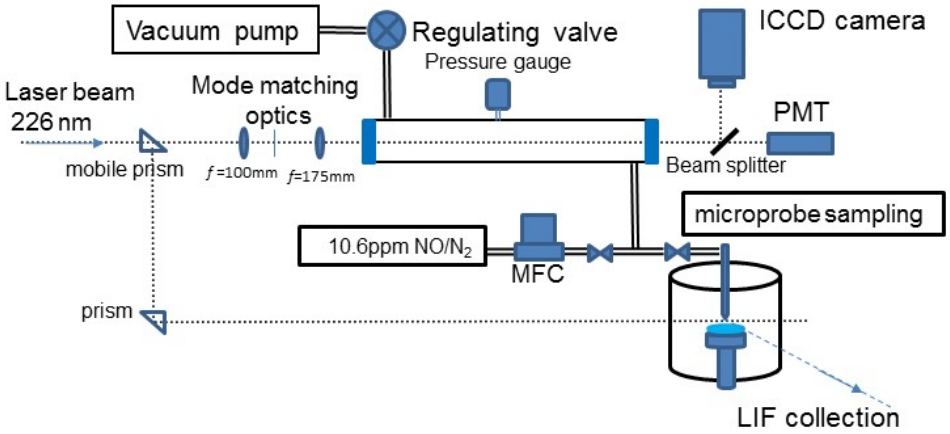

Figure 2. Sketch of the experimental setup with the CRDS cell including the system for injecting the standard gas, the gas sampling through the microprobe, and the arrangement of the LIF setup. The microprobe is withdrawn during in-situ LIF measurements, and the mobile prism is shifted for the ex-situ CRDS measurements.

2.3 Laser techniques

Two laser-based techniques are implemented in this work; in-situ LIF, and ex-situ CRDS. The pulsed laser system consists of a seeded frequency-doubled Nd:YAG laser (Quantel Q-smart) pumping a dye laser (Quantel TDL90+). Wavelengths around 226 nm (for probing NO in the $A^2\Sigma^+$-

$X^2\Pi(0,0)$ band) are provided after doubling the fundamental dye radiation (around 572 nm) which is mixed with the Nd:YAG residual radiation at 1064 nm. The spectral laser bandwidth at 226 nm is estimated to be around 0.12 cm^{-1}.

LIF and CRDS signals are collected through a photomultiplier tube (PMT) (Photonis, XP2020Q) and recorded on a digital oscilloscope (LeCroy HDO4000, 12-bit vertical resolution, 1GHz bandwidth, 1.25 GS/s). During the acquisition of the absorption spectra, the (fundamental) laser wavelength is scanned at a rate equal to 0.25 pm s^{-1} and signals were averaged over 15 laser shots. For the species profile measurements, signals are averaged over 300 laser pulses. Signals from the oscilloscope and the step motor of the dye laser are transferred in real time on a PC, and treated with Labview programs.

2.3.1 In-situ LIF

NO species can be measured using in-situ LIF. This well-known technique allows measuring in-situ species in relative mole fraction with a high sensitivity and spatial resolution. The laser beam is introduced unfocused parallel to the burner surface. It is shaped using a pinhole with a diameter of 3 mm and a horizontal slit of 300 µm height in front of the burner enclosure and parallel to the burner surface as shown in **Figure 2**~~**Figure 2**~~. The LIF signal is collected by a two-lenses system (f = 200 and f = 350 mm) and focused on the entrance slit of a 0.5 m monochromator (SpectraPro 2500i). The entrance slit (450 µm width, 10 mm height) is parallel to the laser axis. The volume of measure has been estimated to be 260 µm height, 3 mm depth and 6.7 mm long. Its size was chosen to ensure the highest signal/noise ration while guaranteeing that the species gradient is not altered. The output slit is adjusted to obtain a collection bandwidth of 9 nm, centered at 246 nm in order to collect the complete A-X(0-2) vibrational band of NO.

The relative NO concentration profiles are obtained by prompt-LIF in the linear regime of fluorescence according to Eq. (1). The prompt-LIF signal (S_{LIF}) is measured at the peak value of the temporal LIF signal. Measurements are performed under constant laser energy (I_L). The variations of the fluorescence quantum yield (Φ) along the HAB are found negligible. The LIF signal is proportional to the rotational population of the laser-probed level. Its conversion into relative concentration of NO, $N_{NO,r}$, is achieved by dividing the signal by the Boltzmann factor $f_B(J'',T)$, easily calculated using the experimental temperature data. In order to limit the impact of the temperature uncertainties on the Boltzmann factor calculation, NO is excited via the $Q_2(26.5)$ line (at 225.58 nm) for in-situ LIF measurements. Indeed, the temperature dependency of the Boltzmann factor of this rotational level in the flame temperature range is limited.

$$S_{\mathrm{LIF}} = N_{\mathrm{NO,r}} f_{\mathrm{B}}(\mathrm{J}'', T)\Phi I_L \qquad \text{Eq. (1)}$$

From the ideal gas law, the relative concentration of NO is converted into the relative mole fraction $X_{NO,r}$. In the case of NO species, the relative mole fraction can be converted into the absolute value X_{NO}, using the LIF response to small known amounts (same order than the expected native NO) of NO added in the premixed gases [50–53]. The NO standard addition method relies on the main assumption that there is no NO-reburning in the flame, and that the dilution effect due to the variation of the total mole number along the flame is negligible..

The temperature is determined from NO-LIF thermometry. Small amounts of NO is substituted to the nitrogen diluent, and NO species is excited in the (0,0) vibrational band at around 225 nm. The laser wavelength is scanned from 225.45 to 225.72 nm, and the fluorescence signal is collected at 245 nm along the entire (0,2) vibrational band. The excitation fluorescence spectra collected at different HAB are compared with synthetic spectra in order to determine the temperature of the gases according to the Boltzmann distribution. More details about the method are given in [48,49].

2.3.2 Ex-situ CRDS

The measurements of NO are performed after gas sampling by CRDS in the external absorption cell. The high sensitivity of the CRDS technique relies on the measurement of the rate of absorption of light circulating in a resonant optical cavity. The quasi-plane cavity (39.5 cm long) is ended by two highly reflective mirrors (Layertec GmbH, 25 mm diameter, - 6 m radius of curvature, reflectivity > 0.993). Typically, the empty ring-down decaytime is equal to 200 ns. As shown in **Figure 2**~~**Figure 2**~~, the laser beam is shaped with a system consisting of a 100 µm pinhole aperture and two lenses (f = 100 and f = 175 mm) in order to match approximately the TEM_{00} transverse mode of the optical cavity. At the exit of the cell, a beamsplitter allows reflecting a fraction of the light towards an ICCD camera for controlling the perfect alignment of the cavity as done by Evertsen et al. [44]. The temporal CRD signal is measured from the transmitted light collected by a PMT in front of which a 226-Corion filter is placed. Ring-down decaytimes, τ, are determined from an exponential fitting procedure over 800 ns [20], which corresponds to 4 times the off-resonance decaytime. Using a 12-bit vertical resolution system, the on-resonance decay as low as 130 ns (fitting period/6) can be reasonably measured [54].

The laser wavelength is scanned around the selected absorption transition in order to measure the integrated spectral absorptivity $A(\bar{\nu})$. Then, the absolute species concentration of NO is calculated according to Eq. (2) [45].

$$A(\bar{\nu}) = \int L(\bar{\nu})d\bar{\nu} = (\pi e^2/m_e c^2) f_{J''J'} N_{NO} f_B(J'', T) l_s = \sigma_{pk}(\bar{\nu}_{pk}, T) N_{NO} l_s \qquad \text{Eq. (2)}$$

where $L(\bar{\nu})$ represents the losses per pass (defined by l_s/ ($c \times \tau$) along the absorption length (l_s in cm) in function of the wavenumber ($\bar{\nu}$), c is the light speed, $m_e c^2/\pi e^2$ is equal to 1.13×10^{12} cm^{-1}, $f_{J''J'}$ is the rotational oscillator line strength for absorption, and N_{NO} is the absolute concentration of NO (in molecule cm^{-3}). $\sigma_{pk}(\bar{\nu}_{pk}, T)$ (in cm^2/(molecule cm^{-1})) is the temperature-dependent absorption

cross-section at the wavenumber of the peak transition $\bar{\nu}_{\mathrm{pk}}$. $f_{\mathrm{J"J}}$, is obtained from the radiative lifetime given in [55], and is equal to 8.226×10^{-5}.

Alternatively, the absolute concentration can be directly determined according to Eq. (3)[45]:

$$L(\bar{\nu}_{\mathrm{pk}}) - L(\bar{\nu}_{\mathrm{OFF}}) = \sigma_{\mathrm{pk}}(\bar{\nu}_{\mathrm{pk}}, T) g(\bar{\nu}) N_{\mathrm{NO}} l_s \quad \text{Eq. (3)}$$

where the difference between the losses $L(\bar{\nu}_{\mathrm{pk}})$ and $L(\bar{\nu}_{\mathrm{OFF}})$ is the net loss per pass. They are measured at the peak transition $\bar{\nu}_{\mathrm{pk}}$ and after detuning the laser wavelength ($\bar{\nu}_{\mathrm{OFF}}$, off-resonance), respectively. $g(\bar{\nu})$ is the laser lineshape convoluted with the absorption transition. This approach requires determining the line shape function $g(\bar{\nu})$ which is quite complex. Here, this function being constant in the cell under controlled *p* and *T*, this approach is satisfactory for measuring the relative concentration of the species.

Because the laser bandwidth (0.12 cm^{-1}) is similar to the Doppler linewidth ($\Delta\bar{\nu}_D$ = 0.10 cm^{-1}) of NO at 300 K, the mono-exponential behavior of the ring-down decay can be easily affected with the increase of the absorbance ($\sigma N l$) as shown in [56,57]. To prevent this, the NO absorbance is measured along the $^{S}R_{21}(7.5)$ line (at 225.87 nm) which is weak enough for allowing the measurement of the NO absorbance at room temperature from a single exponential fitting.

3 Experimental results

First of all, the CRDS measurements have been performed with standard gas mixtures (standard S1 and S2) in order to validate the quantification methodology. Then, the full setup is implemented for measuring the NO mole fraction after gas sampling in the flame using both microprobes (P1 and P2).

3.1 Validation of the pulsed CRDS setup

The procedure of quantification by CRDS is validated by introducing the commercial preparations of NO diluted in nitrogen in continuous flowing in the cell, under controlled temperature and pressure

following an approach close to the one implemented for HCN in [58]. First, the standard gas S1 (2001 ppmv NO) is diluted with nitrogen via two MFC connected to the inlet gas lines of the burner setup. The diluted gas is injected in the burner enclosure at room temperature from which it is probed through the microprobe P1. This arrangement allows controlling the mixing efficiency of the gases in the burner inlet line. The pressure in the cell is maintained at 1.33 kPa (10 Torr) and the dilution of NO is varied from 5 to 30 ppmv in N_2. Thus, the NO concentration ranges from 1.6 to 9.7 × 10^{12} molecule cm^{-3}. Second, the standard gas S2 (10.6 ppmv NO) is directly injected into the cell. The NO concentration is varied from 1.5 to 10 × 10^{12} molecule cm^{-3} by changing the pressure in the cell from 0.5 to 4 kPa, independently of the burner setup. In each condition, the integrated spectral absorptivity is measured allowing for determining the absolute concentration using Eq. (2). Figure 3~~Figure 3~~ shows the resulting concentration in function of the known injected concentration of NO in the absorption cell. Regardless of the procedure (dilution of the standard gas S2, or pressure increase of the standard gas S1), the evolution of the measured NO concentrations with the injected ones is identical. This indicates the absence of NO losses in the sampling line or inside the probe tip using a non-reactive mixture of NO/N_2 at room temperature.

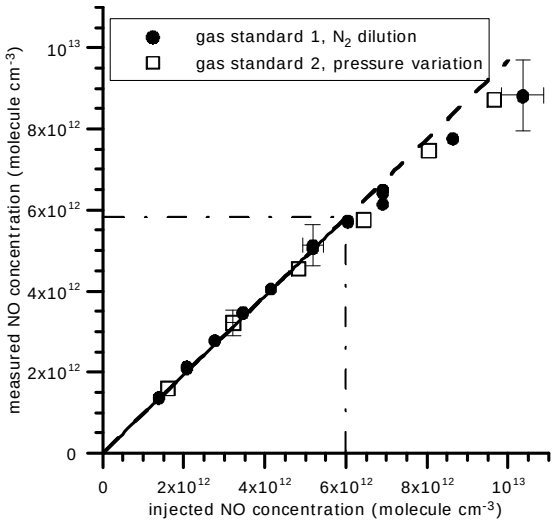

Figure 3. Calibration of NO in the CRD cell at room temperature (300K). The slope of the fitted linear line is equal to 0.97.

When the concentration of NO is lower than 6×10^{12} molecule cm^{-3} (corresponding to a net loss per pass equal to 2×10^{-3} at the peak transition), the measured concentration is found in very good agreement with the injected one (linear fit with a slope equal to 0.97). At higher concentration, the measured value is slightly lower than the injected one. With the increase of the concentration, the absorption coefficient increases, and the ring-down decay is no longer strictly mono-exponential. This yields to an apparent decrease of the measured NO concentration. Because the laser bandwidth is close to that of the NO absorption line, the conditions under which the mono-exponential fitting is appropriate are restricted to a very small range of NO concentration. In order to ensure that the measurements are carried out in the appropriate range of NO concentration (below 6×10^{12} molecule cm^{-3}), the pressure of the probed gas in the cell is maintained at 1.33 kPa, and the maximum mole fraction of NO should not exceed 18.5 ppm at room temperature. The uncertainties for measuring the NO concentration in the CRD cell have been estimated to be ± 14% due to the pressure gauge (0.5% of the full scale, FS), the spectroscopic parameters (2%), and the statistical error for the CRD measurements (6%), additionally of those due to the mixture dilution and preparation (5%).

3.2 Effect of the microprobe in the post-flame

The measurements are undertaken at 20 mm in the flames F1 and F2 (i.e. in the burned gases where the temperature and the NO concentration are constant). The absolute calibration of NO is performed in the flames by LIF or by CRDS. The in-situ LIF measurements are calibrated from the standard addition method by LIF. The gas flow from the standard gas S1 for the NO addition is substituted to the main nitrogen diluent of the flame. The absorption measurements by CRDS are performed after

gas sampling using both microprobes P1 and P2. The measurements carried out in-situ and ex-situ in both flames are detailed below.

3.2.1 In-situ measurements by LIF without probe

The NO prompt-LIF signal after exciting the $Q_2(26.5)$ transition is converted into absolute mole fraction by using the standard addition method detailed in [47,51]. For that, NO is substituted to N_2 in the premixed gases within a small range of mole fractions (0 to 40 ppm) using the standard gas S1 and the same arrangement of the MFC as described before. The maximum added NO mole fraction is low enough to ensure that the NO-reburning is avoided in agreement with [51]. Figure 4~~Figure 4~~ shows the variation of the prompt-LIF signal at HAB = 20 mm in function of the known mole fractions of NO added in the premixed gases. The absolute value of the *x*-intercept is the native NO mole fraction, equal to 10.6 ± 1.1 ppm and 9.6 ± 1.0 ppm in flames F1 and F2, respectively. The overall uncertainty is estimated to be ± 10%, due to the pressure gauge and MFC accuracies (0.5% FS for each apparatus), the standard gas preparation (2%), the linear regression (1%), and the statistical error for LIF measurements (5%).

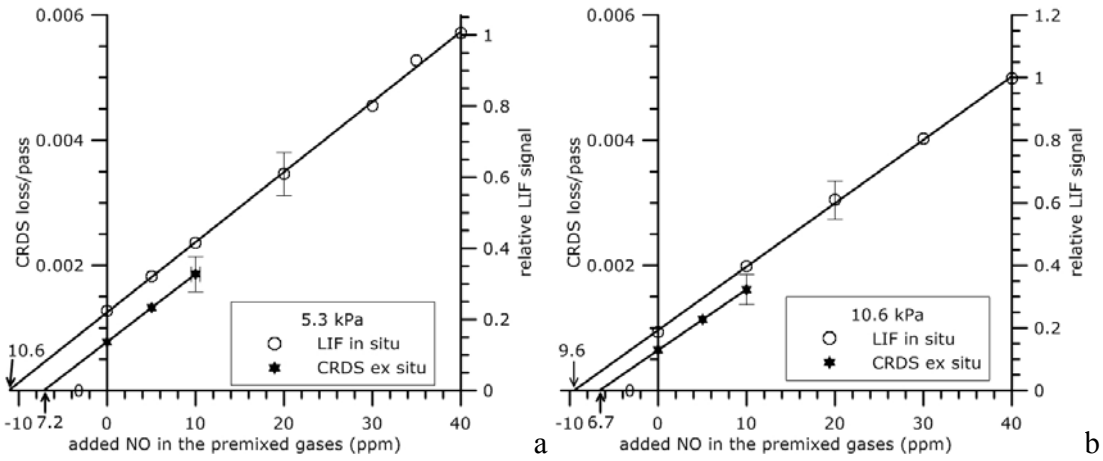

Figure 4. NO calibration at in (a) Flame F1 and (b) Flame F2 from the NO standard addition method (SAM) in the premixed gases (HAB = 20 mm) using in-situ LIF or ex-situ CRDS with the microprobe P1.

3.2.2 Ex-situ measurements using CRDS after gas probe sampling

For the ex-situ measurements, gases are continuously sampled from the flames at HAB=20 mm. The two microprobes (P1 and P2) are tested. The absolute concentration of NO is obtained from the integrated spectral absorptivity measurements by CRDS along the $^{S}R_{21}(7.5)$ transition according to Eq. (2). It is converted into absolute mole fraction of NO knowing the temperature (room *T*) and pressure (p = 1.33 kPa) in the cell. In the flame F1 and with the microprobe P1, the measured mole fraction of NO after gas sampling is equal to 6.7 ± 0.7 ppm which is lower than the value obtained by LIF calibrated by the NO addition method. With the microprobe P2, the NO mole fraction is determined equal to 11.4 ± 1.1 ppm, in very good agreement with the value obtained by LIF. In the flame F2, the absolute mole fraction of NO is equal to 6.2 ± 0.7, and 9.3 ± 0.9 ppmv after probing the gas with the microprobe P1 and P2, respectively. This last value is in a good agreement with the one determined by LIF (see **Table 2**). The uncertainty is estimated to be equal to 9%, due to the pressure gauge (0.5% FS), 6% for the experimental standard deviation and 2% for the spectroscopic data.

Further investigations are undertaken with the microprobe P1 to identify the source of the discrepancies between the absorptivity measurements performed with the two microprobes. First, the standard addition method (with the standard gas S1 in the premixed gases) is applied to the CRDS measurements as so as during the LIF calibration. The pressure in the absorption cell is maintained at p = 1.33 kPa, and the net losses per pass due to the NO absorption is determined at the peak of the $^{S}R_{21}(7.5)$ transition using Eq. (3) for each amount of NO added. **Figure 4**~~**Figure 4**~~ shows the variation

of the losses per pass in function of the NO added in the premixed gases of the flames F1 and F2. Here, the NO addition is limited to 10 ppm to ensure that the CRD measurements are appropriately performed using a mono-exponential fitting (and the net losses per pass are effectively lower than 2 $\times 10^{-3}$ as shown in **Figure 4**~~**Figure 4**~~). The mole fraction of NO in the flame F1 is equal to 7.2 ± 1.1 ppm, in good agreement with the value obtained directly from the integrated spectral absorptivity in the neat flame (6.7 ppm). In Flame F2, the mole fraction of NO is equal to 6.7 ± 1.0 ppm from the standard addition method, and 6.2 ± 0.7 ppm from the direct absorption measurement in the neat flame. The overall uncertainty is estimated to be ± 15% (for the CRDS measurements performed with NO addition method). The NO mole fractions measured after sampling with P1, using the SAM method and the method based on the neat NO measurement from the integrated absorptivity are in very good agreement. Furthermore, the LIF and CRDS signals increase linearly with the NO addition in different conditions of NO injection.

Additional tests are performed in flame F1 with the microprobe P1. First, the residence time of the gas in the probe is varied by acting on the pressure in the cell from 1.0 to 2.7 kPa. The same value of the NO mole fraction is measured, indicating no effect of the residence time on quenching reactions in agreement with [30,31]. Second, small amounts of NO are added to the sampling line in-between the absorption cell and the microprobe. No evidence of NO losses in the sampling line can be seen. The results are gathered in **Table 2**.

Table 2. NO mole fractions (in ppm) measured in the burned gas of stoichiometric $CH_4/O_2/N_2$ flames stabilized at p = 5.3 and p = 10.6 kPa, by in-situ LIF from the standard addition method (SAM) and by ex-situ CRDS after gas sampling through the microprobe P1 or P2. With the microprobe P1, the CRDS measurements are also calibrated from SAM as done by LIF.

	LIF, SAM	CRDS, P1	CRDS, P1 SAM	CRDS, P2
Flame F1 (5.3 kPa)	10.6±1.1	6.7±0.7	7.2±1.1	11.4±1.1
Flame F2 (10.6 kPa)	9.6±1.0	6.2±0.7	6.7±1.0	9.3±0.9

In the burned gases (HAB=20 mm) and for both pressures, the values of the NO mole fractions determined by CRDS after gas sampling with the microprobe P1 are found 40% lower than the values measured with the microprobe P2. However, the absolute mole fraction of NO measured by CRDS with the microprobe P2 is found in very good agreement with the value determined from the NO addition by LIF. Furthermore, the NO mole fractions determined using CRDS measurements with the microprobe P1 either directly from the integrated spectral absorptivity of from the standard addition method are found in very good agreement together. This suggests that the NO-reburning and the dilution effects (due to the total mole number variation in the flame) which could affect the standard addition method is negligible. This also indicates that the NO losses are very weak inside the microprobe P2 and in the sampling line, and that the perturbations induced by the microprobe P2 in the burned gases of the flame are negligible. By contrast, the perturbations induced by the microprobe P1 in the gas sampling carried out in the burned gases are significant. At this stage, no explanation could be found. In the following, we present the NO profiles measured in function of the HAB so as a detailed kinetic analysis to attempt to elucidate this observation.

3.3 Effect of the microprobe along the HAB

The in-situ and ex-situ NO mole fraction profiles are measured in function of HAB after exciting the molecule at the peak of the selected transition ($Q_2(26.5)$ in the flame or $^{S}R_{21}(7.5)$ in the CRD cell). In order to highlight the perturbation induced by the microprobes on the shape of the NO profiles, the discussion first focusses on the comparison between the normalized NO profiles. The in-situ relative

LIF profiles are corrected for the Boltzmann factor and the variation of the temperature along the flame axis according to Eq. (1). After gas sampling, the NO mole fraction profiles are measured from the measurement of the net losses per pass according the Eq. (3). The relative NO mole fraction profiles obtained in both flames using the three methods are normalized at HAB = 20 mm as shown in Figure 5~~Figure 5~~.

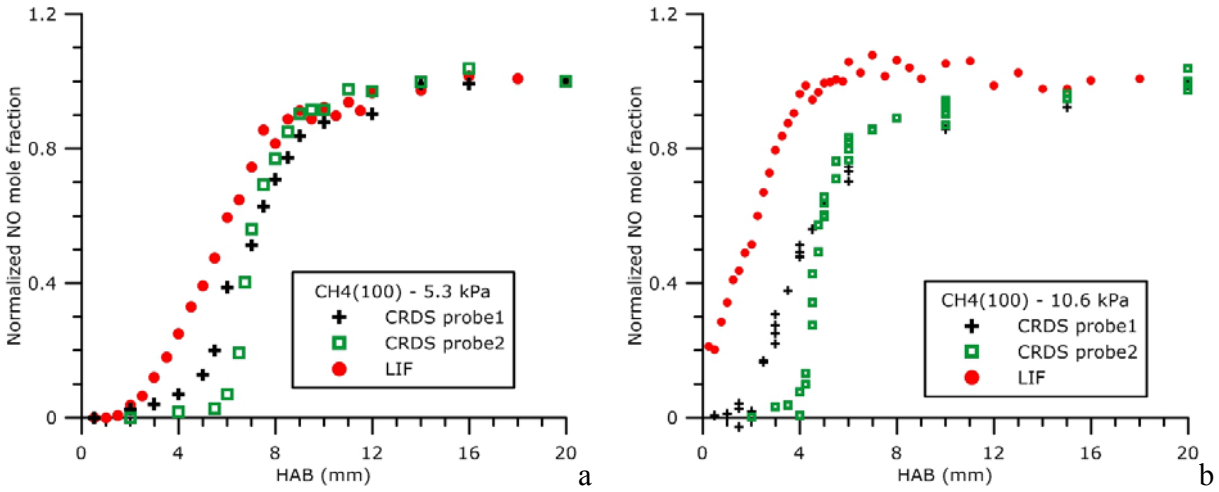

Figure 5. Normalized NO species profiles in function of HAB in stoichiometric $CH_4/O_2/N_2$ flames obtained either by in-situ LIF or after gas probe sampling by CRDS. (a) p = 5.3 kPa, and (b) p = 10.6 kPa.

Whatever the pressure of the flame, the shape of the relative NO profiles obtained by using three experimental approaches differs one from each other as shown in Figure 5~~Figure 5~~. As expected, by increasing the pressure, the gradients of the NO species profiles are steeper and closer to the burner surface. Clearly, the NO profiles obtained after probe gas sampling are shifted downstream compared to the unperturbed profiles obtained by in-situ LIF. The shape of the NO profile obtained by CRDS is less disturbed by using the microprobe P1 than the microprobe P2 (compared to the unperturbed LIF

profile). The gradient of the NO profile obtained by CRDS with the microprobe P2 is about 1.8 times steeper than the ones observed with the microprobe P1 or by LIF. This indicates that the flame is spatially less perturbed by the sharp tip. However, both microprobes induce a shift of the reaction zone. Indeed, the inflection points of the NO profiles at p = 5.3 kPa obtained by CRDS are shifted downstream by 2.2 and 2.6 mm by using the microprobes P1 and P2, respectively. At p = 10.6 kPa, the shifts are even greater: 3.8 and 4.8 mm, with P1 and P2, respectively. This higher perturbation arises from the closer proximity of the flame to the burner surface with the pressure increase. The present observations are in agreement with those reported with a sampling cone [5], indicating that the gradients of the species profiles steepen and are further shifted downstream with the increase of the tip angle.

Second, each profile is independently converted into absolute mole fractions using the absolute value measured at HAB = 20 mm by LIF and by CRDS after gas sampling through the microprobes P1 and P2 described above (see **Table 2,** columns 2, 3 and 5, respectively). The absolute NO mole fraction profiles are compared together in Figure 6~~Figure 6~~. Note that in Flame F1, the NO profile obtained in the present work are found in very good agreement with the one previously presented in [42].

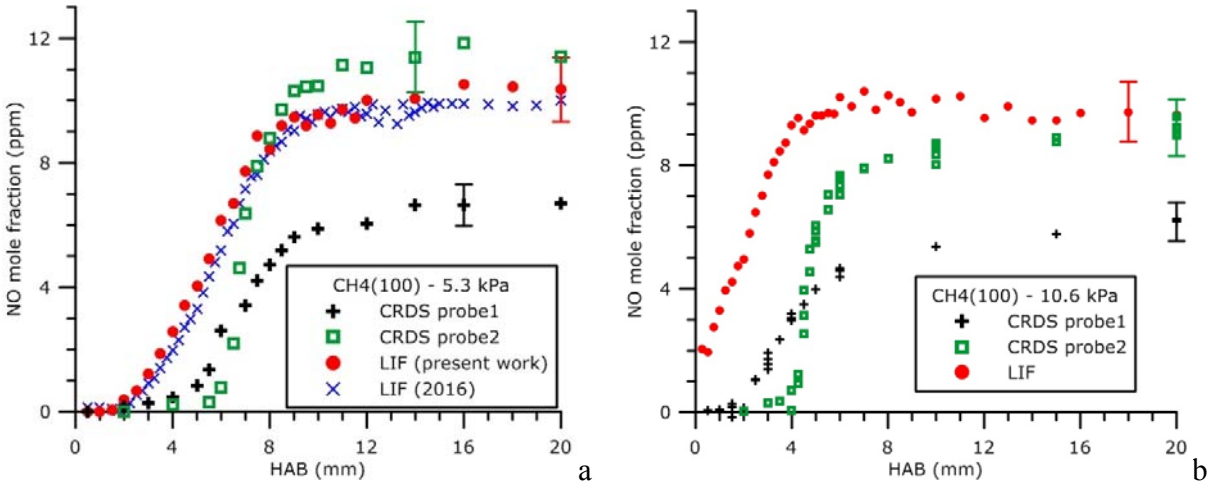

Figure 6. Absolute NO mole fraction profiles in function of HAB in stoichiometric $CH_4/O_2/N_2$ flames obtained either by in-situ LIF or after gas probe sampling by CRDS. (a) p = 5.3 kPa, and (b) p = 10.6 kPa.

Figure 6~~Figure 6~~ shows clearly the perturbations generated by the microprobes used in the present work compared to NO profiles measured in situ by LIF in absence of the probe. The disturbances are limited to a shift of the gradient NO profile by around 1 mm using the thinner microprobe P1, while the steepen of the gradient using the microprobe P2 may indicate that the flame is more attached to the tip than it was visible. However, the absolute mole fraction of NO measured by CRDS after gas sampling through the thinner microprobe P1 indicates a deterioration of the gas sample composition with a loss of 40% of its nominal value measured by in-situ LIF. On the contrary, the gas sample composition is not degraded when it is probed with the larger microprobe P2.

4 Modeling and discussions

In the burned gases area where the temperature and the NO concentration reach a plateau, the present work indicates clearly an important discrepancy between the ex-situ measurements performed with two different microprobes. In one of the two cases, the ex-situ results are found in very good agreement with the in-situ measurement using LIF (without the microprobe). The microprobes differ by their tip cone angle, their area ratio and their surface/volume ratio, which can affect the residence time of the gases in the tip of the microprobe, the efficiency of the quenching of chemical reactions, the surface reactions or the frictional chocking [25,26,29–31]. The reactivity inside the probes is simulated considering the residence time of the sampled gas and the surface/volume ratio, by using the Senkin module at constant temperature. Then, the disturbance of the temperature profiles is examined by computing with Premix, the NO profiles in the flame with or without the presence of the probe. The calculations are performed using the Chemkin-II code with the GDFkin3.0_NOMecha2.0 mechanism

[42]. Under the present conditions of pressure equal to 5.3 kPa (and 8.6 kPa) in the flame F1 (and F2) and to 1.3 kPa in the absorption cell, the probe suction described in Refs. [12,13] is assumed weak. Thus, the analysis has been conducted with the assumption that the probe samples the gas just in front of its hole.

4.1 Possible reactions inside the microprobe

For the flame F1 stabilized at p = 5.3 kPa and with a pressure in the absorption cell equal to p = 1.33 kPa, the volumetric flow rate of the sampling gas is measured at 6.54 sccm at HAB = 20 mm, as explained in the Supplementary Materials. It is identical with both microprobes which have the same tip opening of 200 µm in diameter. This corresponds to a mass flow rate in the probe equal to around 1.6 µg s^{-1}, which is in agreement with the recommendations given by Fristrom and Westenberg [23]. Note that the gas mass flow rate in the flame is equal to 98.4 mg s^{-1}. Thus, the mass flow rate decreases by a factor of about 6×10^4, indicating a rapid expansion of the gas in the probe.

Considering the geometric characteristics of both microprobes as summarized in **Table 1**, the resulting speed of the gas in the section 1 of the microprobe is about 2.3 times greater in the microprobe P1 compared to P2. Of course, the volumetric flow rate as the gas speed depend on temperature inside the probe. In a first approximation, if the pressure drops suddenly from the pressure of the flame down to 1.33 kPa and the temperature is assumed to decrease linearly in the tip from the burned gases temperature down to 300 K where it remains constant in the first cylindrical section (section 1 drawn in **Figure 1**~~**Figure 1**~~), the residence time of the gas sample is estimated to be 1.3 ms and 3.0 ms (respectively for P1 and P2). Because the temperature increases with the HAB, the volumetric flow rate of the sampling decreases, and the residence time increases. In the present work, no efforts have been undertaken to work at constant residence time along the HAB. The above-mentioned values of the residence time are estimated for gas sampled at HAB = 20 mm.

Because the surface/volume ratio of the microprobe P1 is 1.5 times greater than that of the microprobe P2 (**Table 1**), the surface reactions are certainly favored in the microprobe P1. However, the larger S/V ratio is compensated by the gas velocity (residence time) in the microprobe P1 which is 2.3 times greater (lower) than that in the microprobe P2.

4.1.1 Gas-phase reactions

In order to estimate the effect of the possible gas-phase reactions inside the microprobes (including the tip and the section 1), simulated calculations of the NO mole fractions are performed considering a 0-D reactor at constant temperature as function of the residence time by using the Senkin module of the Chemkin-II code. The input species mole fractions are initially calculated with the Premix module for the unperturbed flame F1 at HAB = 20 mm. The species whose mole fractions is lower than 0.5 ppm are neglected.

If the quenching is fully efficient, all short-lived and radical species are quenched, yielding to a perfectly frozen chemical system. If not, the sampled stable species will react in the gas phase, with the remaining small fractions of these species (such as OH, O or H). The computations are performed at 300 K by considering that a small fraction of the species (OH, O, H) present in the flame persists together with all the stable species (i.e. H_2, O_2, CO, CO_2, H_2O, N_2, and NO) at the inlet of the probe. The simulated NO mole fractions decrease as function of the residence time but in a limited range of a few percent. The NO decrease is all the more important that the remaining fractions of (OH, H and O) are important as shown in **Figure 7**~~**Figure 7**~~. Even if 10% of these atoms and radical are remaining, the NO decrease after 1.3 ms does not exceed 3% of the initial value.

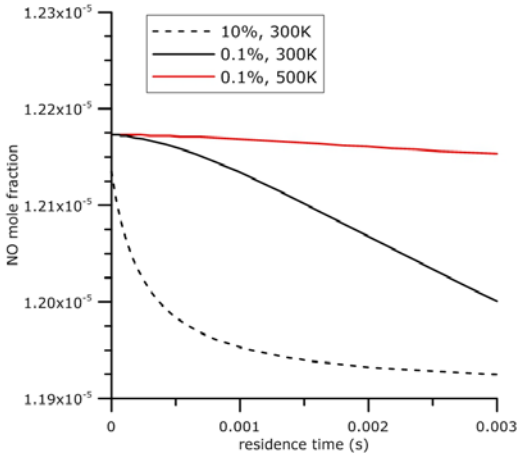

Figure 7. Variation of the NO mole fraction in function of the residence time in a 0-D reactor at T = 300 K or 500 K. The initial conditions are imported from the Premix output values at HAB = 20mm for the flame F1 with a remaining fractions of O, H and OH equal to 0.1% or 10.0%.

At 300K, with 0.1% of the mole fractions of O, H and OH present in the flame remaining inside the probe, the NO rate-of-progress analysis shows that NO is consumed through two reactions: NO + OH +M ⇌ HONO +M and NO + HO_2 ⇌ NO_2 + OH, and is formed through the reaction NO_2 + H ⇌ NO + OH. It appears that the HO_2 radicals (initially absent in the input simulation) are formed via the reaction H + O_2 +M ⇌ HO_2 +M (consumption of H-atoms), and consumed via the reactions HO_2+OH ⇌ H_2O+O_2 (consumption of OH) and H+ HO_2 ⇌ H_2O+O (formation of O-atoms). OH radicals are consumed through CO+OH ⇌ CO_2+H (formation of H) and formed via H+HO_2 ⇌ OH+OH. The O-atoms are also consumed through the reaction CO+O+M ⇌ CO_2+M. The O-atoms and OH radical mole fractions decrease, the H-atoms mole fraction first increases and decreases. The HO_2 mole fraction increases continuously up to 5 ppm after 3 ms and the NO_2 mole fraction up to 0.16 ppm.

These gas-phase reactions cannot explain the NO losses observed during the gas sampling with the microprobe P1 where the residence time is assumed to be equal to 1.3 ms.

All these atom- and radical-molecule reactions require very weak energy. If the temperature inside the probe is equal to 500 K, the NO consumption is lower than that at 300 K. Successful flame sampling is more dependent on a rapid pressure drop with destruction of radicals on the probe wall, rather than a rapid temperature drop [59].

4.1.2 Recombination reactions at the inner wall

From the ROP analysis, the recombination reaction $H + O_2 + M \rightleftharpoons HO_2 + M$ turns out to be very important, indicating that the wall-recombination (third-body) can be non-negligible. In order to examine this point, this reaction and two other termolecular reactions ($NO + OH + M \rightleftharpoons HONO + M$, and $CO + O + M \rightleftharpoons CO_2 + M$) have been artificially modified in order to increase the contribution of the recombinations at the wall. The calculations show that whatever the wall-reactions contribution, the residence time inside the microprobe is too short to see any significant modification of the NO mole fractions, in agreement with Kaiser et al. [31].

4.1.3 Heterogeneous surface reactions inside the probe

Heterogenous reactions may occur at the surface as described for quartz reactor (silica-based) in [60–62]. Allen [29] described that NO quickly react with O-atoms at the quartz wall, yielding NO_2. If the aerodynamic quenching in the probe is not efficient, the remaining O-atoms will react with NO_2 yielding back NO. Kramlich and Malte [25] computed the species variation in the probe along the axis by considering wall reactions for the atoms recombination and gas-phase reactions. The rates of the surface reactions are increasing with decreasing the area ratio (increasing the surface/volume ratio), yielding to a faster recombination of O and H atoms into O_2, H_2 and HO_2. The conversion of NO into NO_2 is mainly explained by the reaction between NO and HO_2.

The recombination probability factors reported for atomic H [63], O [64] and N [65] are similar, and the one for NO is 3 or 4 orders of magnitude lower [61]. In the present work, heterogeneous reactions have been implemented in the modeling by introducing pseudo-first-order reaction as performed by Glarborg et al. [66] to simulate the NO conversion in a quartz plug-flow tube. Due to the very limited residence time in the probe (typically less than 3 ms), the heterogeneous reactions are found to be negligible.

4.2 Temperature perturbations

The in-situ temperature profiles have been measured by using NO-LIF thermometry and are shown in **Chart 1** (panels a, b) for the two flames. Using these profiles, the simulated NO profiles are found in very good agreement with the experimental NO profiles measured by in-situ LIF as shown in **Chart 1** (panels c, d).

4.2.1 Effect on the NO mole fraction profiles

If the disturbance effects of the microprobe were restrained to the distortion lines of the temperature only, the thinner microprobe P1 should produce less perturbation along the HAB than the microprobe P2. In order to identify the sole temperature perturbation due to the microprobe (heat sink and streamline distortion), 1D simulations have been performed using the Premix code. For each microprobe and in each flame, the input temperature profile is manually modified starting from the experimental profile in order that the simulated NO profile matches the experimental ones obtained after gas probe sampling. This corresponds to the perturbed temperature profile. The resulting simulated NO profiles are shown in **Chart 1** (panels c-f), and compared to the experimental profiles obtained after gas sampling.

Chart 1 (panels a-b) shows the experimental unperturbed and the deduced perturbed temperature profiles in each flame. The gradient of the modified temperature profile used as input data for

simulating the NO profile obtained with the microprobe P1 is close to that of the unperturbed profile. On the contrary to simulate the NO profile measured with the microprobe P2, the gradient of the perturbed temperature profile is much steeper and seems unrealistic. Even with a step of 800 K in 100 μm in the gradient, the simulated NO profile is not as steep as the experimental profile. Due to convergence and solver limitation of the computations, it is not possible to further increase the temperature gradient to match the simulated NO profile as shown in **Chart 1** (panels a-b). Also, the onset of the temperature gradient is widely shifted downstream by around 4 mm. To interpret this inability to simulate the NO profile measured after gas sampling through the microprobe P2, it is suggested that it can be due to the attachment of the flame to the probe tip when it is teared downstream the reaction zone. A slight attachment in the reactive zone was indeed observable. Thus, the distortions of the lines of equal temperature and species in the flow field of the flame are limited with the microprobe P1 compared to those induced in presence of the microprobe P2.

In the following, the discussion of the modified temperature profiles is limited to the ones used to simulate the NO profiles with the microprobe P1 in both flames. In the burned gases (HAB = 20 mm), the temperature measured without the microprobe reaches 1860 K and 1690 K in flames F1 and F2, respectively. In presence of the microprobe P1, the calculated perturbed values decrease by 170K down to 1690 K and 1520 K in flames F1 and F2, respectively. The cooling effect, estimated from the simulation above, is much lower than that observed by Hansen et al. [14,15] using X-Ray fluorescence in presence of a large cone, but close to the value of 150 K with a microprobe reported by Tran et al. [37]. Also, the temperature gradient is shifted by about 1.5-2 mm downstream in presence of the probe. The temperature decrease brings the calculated NO mole fractions 35% lower than the experimental values obtained without the probe, but in agreement with the experimental data measured after gas sampling (see **Table 1**).

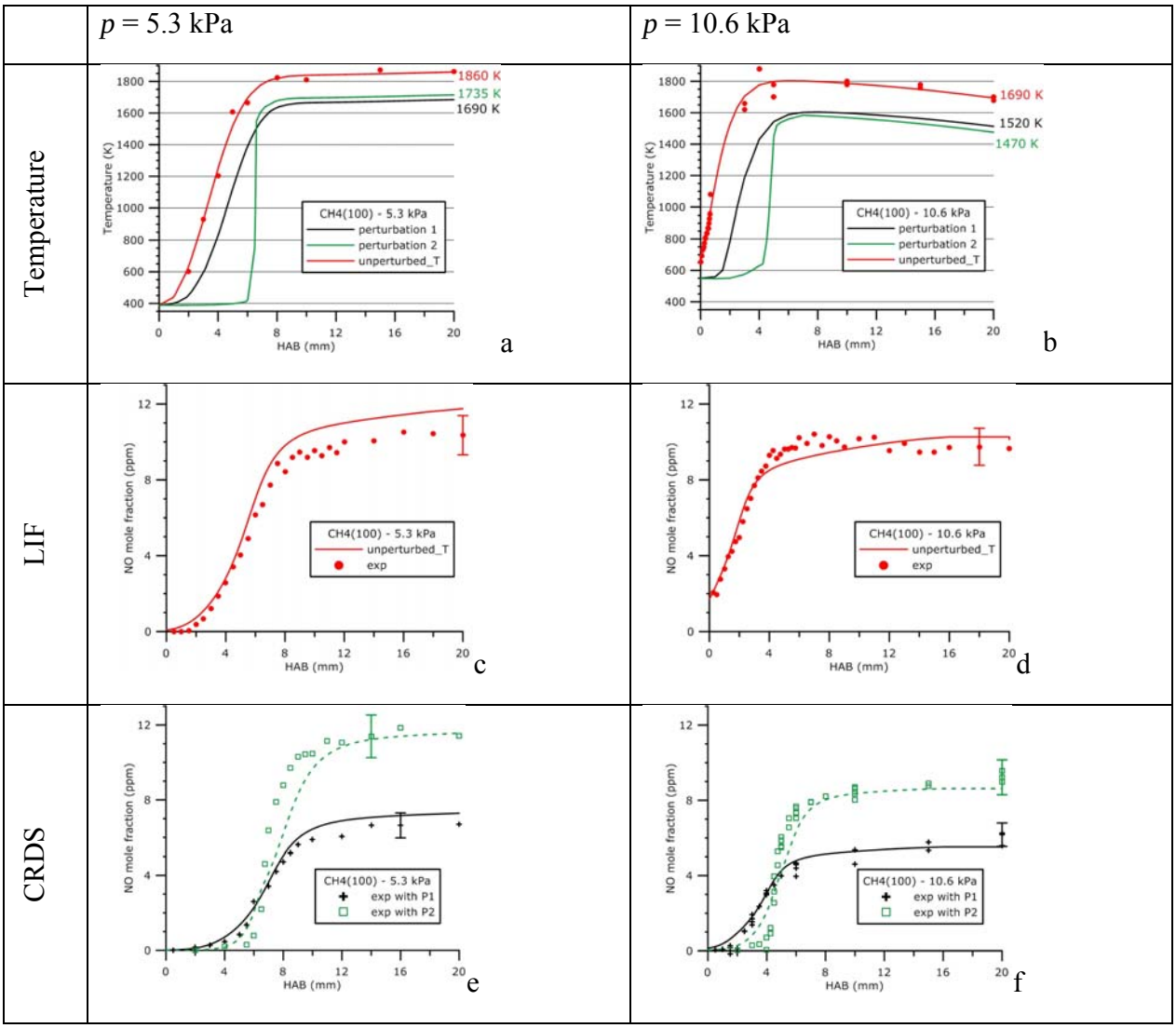

Chart 1. Comparison between the simulated (curves) and the experimental (symbols) NO profiles measured in the $CH_4/O_2/N_2$ flames F1 (c,e) and F2 (d,f). Panels (c,d) by in-situ LIF, Panels (e,f) by CRDS using the microprobes P1 and P2. The colored curves represent the simulated NO mole fraction profiles using the unperturbed or the perturbed temperature profiles shown in panels (a,b). See text.

The present data obtained with the microprobe P2 in the burned gas are in very good agreement with the unperturbed NO mole fractions even though the perturbations generated by the microprobe P2 in the flame front are important. Zabielsky et al. [27] or Li et al. [28] have also determined small

variations of the NO mole fractions measured in the burned gas using in-situ and ex-situ after gas sampling with microprobes. The orifice diameter of the water-cooled quartz probe in [27] is 0.6 mm. The tip opening of the uncooled quartz probe used in [28] is 1 mm in diameter, and the half-angle of the tip is about 25-30°. These satisfactory results have only been obtained in the burned gases. This also raises the question of whether the magnitude of the disturbance of the probe depends on the species being measured.

4.2.2 Potential effect on other species

The HCN mole fraction profile has previously been measured in the flame F1 after gas probe sampling with the microprobe P1 [58]. Figure 8~~Figure 8a~~ shows the comparison of the experimental HCN mole fraction profile measured by *cw*-CRDS using the microprobe P1 with the simulated profiles obtained by using either the unperturbed or the perturbed temperature profile. The experimental profile peaks 0.6 mm after the unperturbed simulated profile, and 1 mm before the perturbed profile. The simulated peak mole fractions by using both temperature profiles are found in good agreement with the experimental determined within an overall uncertainty equal to 20%. As the CH radical is a key species for the prompt-NO formation, **Figure 9b** presents the comparison of the experimental CH profiles and the simulated profiles. The experimental CH profiles were previously measured in-situ using LIF and CRDS [42]. The simulated CH peak position is found in very good agreement with the simulated peak location using the experimental temperature profile. The peak mole fraction of the simulated CH profiles using the perturbed temperature profile is shifted 1.6 mm downstream and decreases by 20% in comparison with the simulated profile using the experimental temperature profile. This change is close to the one observed for HCN, which is also an intermediate species in-between CH and NO.

Calculations of few main stable species (including intermediate species as the C2-hydrocarbons and HCN, and product species as NO, CO and CO_2) have been performed with the two temperature profiles in the experimental conditions of the flame F1. As expected with the perturbed temperature profile, the peak species profiles are shifted towards the burned gas by around 1.5 mm as is the shift of the temperature profile . The simulated peak species mole fraction values are reported in **Table 3**. The predicted NO and HCN mole fractions decrease by 38% and 23%, respectively. But, the CO and CO_2 mole fractions increase by 2 and 6%, respectively. The C2-hydrocarbons peak mole fractions also increase with the decrease of temperature from the unperturbed to the perturbed profiles. The variations calculated for C_2H_4 and C_2H_6 are much greater than for C_2H_2. Interestingly, the comparison between the mole fractions measured either by GC with a microprobe or by MBMS with a cone as performed by Liu et al. [36], reveals also discrepancies for C_2H_4 and C_2H_6 twice higher than for C_2H_2.

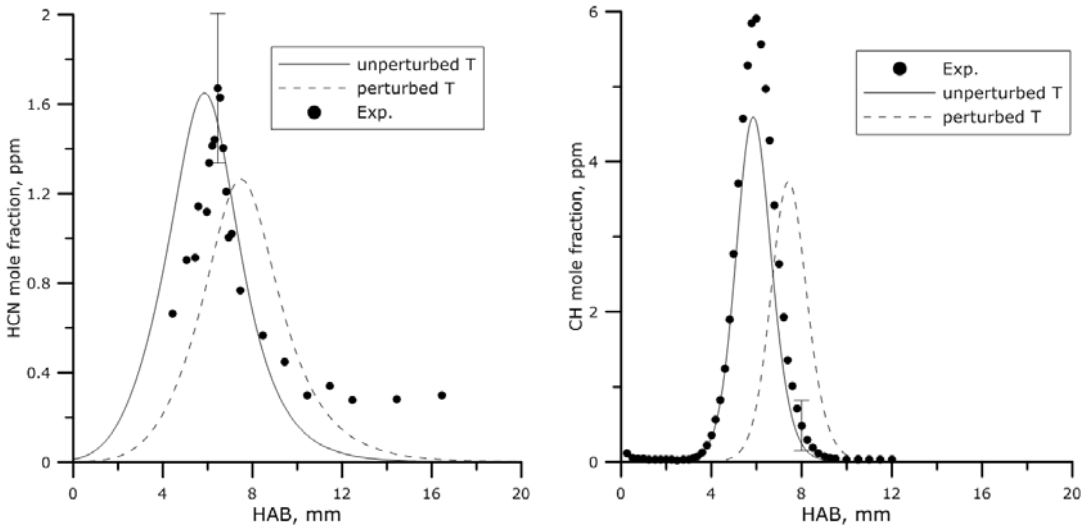

Figure 8. HCN and CH mole fractions profiles in flame F1. Symbols represent the experimental data obtained (a) of HCN after gas sampling with the microprobe P1 [58] and (b) of CH using in-situ LIF [42].

The lines represent the simulated profile obtained with the unperturbed temperature profile (solid), and with the perturbed temperature profile in presence of the microprobe P1 (dashed).

Table 3. Simulated peak mole fractions of few species using the experimental temperature profile (unperturbed T) or the modified temperature profile in order to match the perturbed NO profile obtained with the probe P1.

Species	Unperturbed T	Perturbed T	variations
NO [a)]	11.8×10^{-6}	7.33×10^{-6}	-37.9%
HCN	1.63×10^{-6}	1.26×10^{-6}	-22.7%
C_2H_2	2.32×10^{-4}	2.40×10^{-4}	+3.5%
C_2H_4	7.58×10^{-4}	8.59×10^{-4}	+13.3%
C_2H_6	7.04×10^{-4}	8.33×10^{-4}	+18.3%
CO	5.48×10^{-2}	5.58×10^{-2}	+1.8%
CO_2 [a)]	6.58×10^{-2}	6.96×10^{-2}	+5.7%

a) In the burned gases

These calculations show that the thermal perturbation affects differently the intermediate species and the product species. The NO species are among the species which are the most affected by the temperature disturbance due to the probe.

5 Conclusions

In the present work, the NO profiles in stoichiometric low-pressure $CH_4/O_2/N_2$ flames have been measured by using either in-situ LIF or ex-situ CRDS techniques. The in-situ NO-LIF profile is converted into absolute mole fractions from the standard NO addition method. The ex-situ

measurements are undertaken after probing the gases from the flame through uncooled quartz microprobes. Two shapes of microprobes have been examined; the tip half-angle is estimated to be 3.3° and 7.9° for the microprobe P1 and P2, respectively. Gases are sampled in the same conditions of flow rate and pressure inside the probe, and analyzed in an external absorption cell where the measurements have been performed by CRDS.

The relative profiles of the NO mole fraction are measured by in-situ LIF and after gas sampling with the two microprobes by CRDS. NO profiles obtained after probe sampling are shifted downstream. The shift is all the more important that the tip angle of the microprobe is large. In this case, the NO profile presents a very steep gradient. The shape of the NO species profile obtained with the sharp angle probe is close the NO profile measured using in-situ LIF, indicating that the perturbations are limited along the HAB when the gas sampling is carried out with the microprobe P1.

However in the burned gases, the NO mole fraction values obtained by using CRDS after probing the gases through the microprobe P1 are found 40% lower than the values measured either in-situ by LIF or ex-situ but with the microprobe P2. Additional tests have been undertaken in the present study to understand the experimental source of this discrepancy.

Modeling computations have been performed in order to examine the surface reactions (wall-reactions and heterogeneous reactions) and the temperature perturbation. The estimated residence time (~3ms) is too short, and surface reactions are too slow to induce any disturbance of the sampled gas (at least regarding the NO species). We finally explored whether the temperature perturbation could be a source of disturbance. Based on the temperature profiles measured in-situ by NO-thermometry LIF, the simulated NO profiles are found in very good agreement with the experimental profiles obtained by in-situ LIF. These unperturbed temperature profiles have been then modified in order to

find a good agreement between the new NO simulated profiles and those measured after gas sampling by CRDS. The profiles obtained with the larger probe are too steep to be retrieved from calculations. This indicates that in presence of this microprobe, the flame may remain attached to the probe. On the contrary with the smaller tip angle, it is possible to find a modified temperature profile from which the resulting NO profile matches very satisfactorily the experimental profile. The perturbed temperature in the burned gases is mitigated by 150 K compared to the unperturbed one, and the gradient location is moved downstream by about 1 mm but with a conservative slope. It seems that a small tip angle limits the perturbations of the shape of the species profiles but at the expense of the absolute mole fraction measurements which are underestimated.

To better understand the perturbation, further works dedicated to the NO species and temperature profiles measurements using in-situ LIF in presence of the microprobe will be necessary in order to describe the microprobe perturbation in between the burner surface and the tip when varying their relative distance. Such measurements were performed in the past but in presence of large cone [6–8,21]. The temperature disturbance has also been characterized in presence of a smaller cone [67]. These measurements are rather difficult to carry on. It is for instance tricky to estimate the actual position and size of the gas volume sampled with the microprobe, and the laser beam volume is perturbed close to the tip (light scattering, …). In addition, it would be helpful to investigate the probe perturbation using a CFD simulation as performed by Deng et al. [12] for investigate the disturbance caused by a cone in MBMS experiments.

This work shows that the design of the microprobe should be specified in the literature, especially for NO species measurements. Using gas sampling techniques, it is recommended to measure the profiles of selected species like the C2-hydrocarbons in CH_4-flames using different microprobes in order to characterize the generated perturbations not only along the vertical axis but also to the gas

sample composition. Further investigations on the temperature measurements beneath the tip of the microprobe, and on the chemical reactivity occurring during the sampling in the gas phase and at the wall would be helpful to fully understand the difference between the two microprobes. Extension of this work to atmospheric flames and to flame conditions where the thermal-NO formation is dominant are intended.

Acknowledgments. This work is a contribution to the CPER research project CLIMIBIO. The authors thank the French Ministère de l'Enseignement Supérieur, de la Recherche et de l'Innovation, the Hauts-de-France Region and the European Regional Development Funds for their financial support to this project.

References

(1) Blanco, E. D. L. R.; Peck, J.; Miake-Lye, R. C.; Hills, F. B.; Wood, E. C.; Herndon, S. C.; Annen, K. D.; Yelvington, P. E.; Leach, T. Minimizing Sampling Loss in Trace Gas Emission Measurements for Aircraft Engines by Using a Chemical Quick-Quench Probe. *J. Eng. Gas Turbines Power* **2011**, *133* (7). https://doi.org/10.1115/1.4002665.

(2) Lupant, D.; Pesenti, B.; Lybaert, P. Influence of Probe Sampling on Reacting Species Measurement in Diluted Combustion. *Exp. Therm. Fluid Sci.* **2010**, *34* (5), 516–522. https://doi.org/10.1016/j.expthermflusci.2009.11.004.

(3) Veríssimo, A. S.; Rocha, A. M. A.; Coelho, P. J.; Costa, M. Experimental and Numerical Investigation of the Influence of the Air Preheating Temperature on the Performance of a Small-Scale Mild Combustor. *Combust. Sci. Technol.* **2015**, *187* (11), 1724–1741. https://doi.org/10.1080/00102202.2015.1059330.

(4) Veríssimo, A. S.; Rocha, A. M. A.; Costa, M. Importance of the Inlet Air Velocity on the Establishment of Flameless Combustion in a Laboratory Combustor. *Exp. Therm. Fluid Sci.* **2013**, *44*, 75–81. https://doi.org/10.1016/j.expthermflusci.2012.05.015.

(5) Biordi, J. C.; Lazzara, C. P.; Papp, J. F. Molecular Beam Mass Spectrometry Applied to Determining the Kinetics of Reactions in Flames. I. Empirical Characterization of Flame Perturbation by Molecular Beam Sampling Probes. *Combust. Flame* **1974**, *23*, 73–82. https://doi.org/10.1016/S0010-2180(74)80028-3.

(6) Stepowski, D.; Puechberty, D.; Cottereau, M. J. Use of Laser-Induced Fluorescence of OH to Study the Perturbation of a Flame by a Probe. *Symp. Int. Combust.* **1981**, *18*, 1567–1573. http://dx.doi.org/10.1016/S0082-0784(81)80159-2.
(7) Smith, O. I.; Chandler, D. W. An Experimental Study of Probe Distortions to the Structure of One-Dimensional Flames. *Combust. Flame* **1986**, *63*, 19–29. https://doi.org/10.1016/0010-2180(86)90108-2.
(8) Hartlieb, A. T.; Atakan, B.; Kohse-Höinghaus, K. Effects of a Sampling Quartz Nozzle on the Flame Structure of a Fuel-Rich Low-Pressure Propene Flame. *Combust. Flame* **2000**, *121* (4), 610–624. https://doi.org/10.1016/S0010-2180(99)00176-5.
(9) Smith, O. I. Probe-Induced Distortions in the Sampling of One-Dimensional Flames. *Combust. Flame* **1981**, *40*, 187–199. https://doi.org/10.1016/0010-2180(81)90122-X.
(10) Yi, A. C.; Knuth, E. L. Probe-Induced Concentration Distortions in Molecular-Beam Mass-Spectrometer Sampling. *Combust. Flame* **1986**, *63*, 369–379. https://doi.org/10.1016/0010-2180(86)90006-4.
(11) Skovorodko, P. A.; Tereshchenko, A. G.; Korobeinichev, O. P.; Knyazkov, D. A.; Shmakov, A. G. Experimental and Numerical Study of Probe-Induced Perturbations of the Flame Structure. *Combust. Theory Model.* **2013**, *17* (1), 1–24. https://doi.org/10.1080/13647830.2012.715674.
(12) Deng, L.; Kempf, A.; Hasemann, O.; Korobeinichev, O. P.; Wlokas, I. Investigation of the Sampling Nozzle Effect on Laminar Flat Flames. *Combust. Flame* **2015**, *162*, 1737–1747. https://doi.org/10.1016/j.combustflame.2014.11.035.
(13) Gururajan, V.; Egolfopoulos, F. N.; Kohse-Höinghaus, K. Direct Numerical Simulations of Probe Effects in Low-Pressure Flame Sampling. *Proc. Combust. Inst.* **2015**, *35*, 821–829. https://doi.org/10.1016/j.proci.2014.06.046.
(14) Hansen, N.; Tranter, R. S.; Moshammer, K.; Randazzo, J. B.; Lockhart, J. P. A.; Fugazzi, P. G.; Tao, T.; Kastengren, A. L. 2D-Imaging of Sampling-Probe Perturbations in Laminar Premixed Flames Using Kr X-Ray Fluorescence. *Combust. Flame* **2017**, *181*, 214–224. https://doi.org/10.1016/j.combustflame.2017.03.024.
(15) Hansen, N.; Tranter, R. S.; Randazzo, J. B.; Lockhart, J. P. A.; Kastengren, A. L. Investigation of Sampling-Probe Distorted Temperature Fields with X-Ray Fluorescence Spectroscopy. *Proc. Combust. Inst.* **2018**. https://doi.org/10.1016/j.proci.2018.05.034.
(16) Biordi, J. C. Molecular Beam Mass Spectrometry for Studying the Fundamental Chemistry of Flames. *Prog. Energy Combust. Sci.* **1977**, *3*, 151–173. http://dx.doi.org/10.1016/0360-1285(77)90002-8.
(17) Struckmeier, U.; Oßwald, P.; Kaspert, T.; Bohling, L.; Heusing, M.; Kohler, M.; Brockhinke, A.; Kohse-Höinghaus, K. Sampling Probe Influences on Temperature and Species Concentrations in Molecular Beam Mass Spectroscopic Investigations of Flat Premixed Low-Pressure Flames. *Z. Phys. Chem.* **2009**, *223*, 503–537. https://doi.org/l0.1524/zpch,2009.6049.
(18) Hansen, N.; Cool, T. A.; Westmoreland, P. R.; Kohse-Höinghaus, K. Recent Contributions of Flame-Sampling Molecular-Beam Mass Spectrometry to a Fundamental Understanding of Combustion Chemistry. *Prog. Energy Combust. Sci.* **2009**, *35*, 168–191. http://dx.doi.org/10.1016/j.pecs.2008.10.001.
(19) Egolfopoulos, F. N.; Hansen, N.; Ju, Y.; Kohse-Höinghaus, K.; Law, C. K.; Qi, F. Advances and Challenges in Laminar Flame Experiments and Implications for Combustion Chemistry. *Prog. Energy Combust. Sci.* **2014**, *43*, 36–67. http://dx.doi.org/10.1016/j.pecs.2014.04.004.

(20) Cattolica, R. J.; Yoon, S. S.; Knuth, E. L. OH Concentration in an Atmospheric-Pressure Methane-Air Flame from Molecular-Beam Mass Spectrometry and Laser-Absorption Spectroscopy. *Combust. Sci. Technol.* **1982**, *28* (5–6), 225–239. https://doi.org/10.1080/00102208208952557.
(21) Desgroux, P.; Gasnot, L.; Pauwels, J. F.; Sochet, L. R. A Comparison of ESR and LIF Hydroxyl Radical Measurements in Flame. *Combust. Sci. Technol.* **1994**, *100*, 379–384. https://doi.org/10.1080/00102209408935464.
(22) Saggese, C.; Cuoci, A.; Frassoldati, A.; Ferrario, S.; Camacho, J.; Wang, H.; Faravelli, T. Probe Effects in Soot Sampling from a Burner-Stabilized Stagnation Flame. *Combust. Flame* **2016**, *167*, 184–197. https://doi.org/10.1016/j.combustflame.2016.02.013.
(23) Fristrom, R. M.; Westenberg, A. A. *Flame Structure*, McGraw-Hill.; Friedman, R., Series Ed.; series in advanced chemistry; New York, 1965; Vol. 150.
(24) Heitor, M. V.; Moreira, A. L. N. Thermocouples and Sample Probes for Combustion Studies. *Prog. Energy Combust. Sci.* **1993**, *19*, 259–278. https://doi.org/10.1016/0360-1285(93)90017-9.
(25) Kramlich, J. C.; Malte, P. C. Modeling and Measurement of Sample Probe Effects on Pollutant Gases Drawn from Flame Zones. *Combust. Sci. Technol.* **1978**, *18*, 91–104. https://doi.org/10.1080/00102207808946841.
(26) Colket, M. B.; Chiappetta, L.; Guile, R. N.; Zabielski, M. F.; Seery, D. J. Internal Aerodynamics of Gas Sampling Probes. *Combust. Flame* **1982**, *44*, 3–14. https://doi.org/10.1016/0010-2180(82)90058-X.
(27) Zabielski, M. F.; Dodge, L. G.; Colket, M. B.; Seery, D. J. The Optical and Probe Measurement of No: A Comparative Study. *Symp. Int. Combust.* **1981**, *18*, 1591–1598. https://doi.org/10.1016/S0082-0784(81)80162-2.
(28) Li, B.; He, Y.; Li, Z.; Konnov, A. A. Measurements of NO Concentration in NH_3-Doped CH_4+air Flames Using Saturated Laser-Induced Fluorescence and Probe Sampling. *Combust. Flame* **2013**, *160*, 40–46. https://doi.org/10.1016/j.combustflame.2012.10.003.
(29) Allen, J. D. Probe Sampling of Oxides of Nitrogen from Flames. *Combust. Flame* **1975**, *24*, 133–136. https://doi.org/10.1016/0010-2180(75)90136-4.
(30) Schoenung, M.; Hanson, R. K. CO and Temperature Measurements in a Flat Flame by Laser Absorption Spectroscopy and Probe Techniques. *Combust. Sci. Technol.* **1980**, *24*, 227–237. https://doi.org/10.1080/00102208008952442.
(31) Kaiser, E. W.; Rothschild, W. G.; Lavoie, G. A. Chemical Species Profiles of Laminar Propane-Air Flames. *Combust. Sci. Technol.* **1984**, *41* (5–6), 271–289. https://doi.org/10.1080/00102208408923835.
(32) Bufferand, H.; Tosatto, L.; La Mantia, B.; Smooke, M. D.; Gomez, A. Experimental and Computational Study of Methane Counterflow Diffusion Flames Perturbed by Trace Amounts of Either Jet Fuel or a 6-Component Surrogate under Non-Sooting Conditions. *Combust. Flame* **2009**, *156*, 1594–1603. https://doi.org/10.1016/j.combustflame.2009.03.006.
(33) Lefkowitz, J. K.; Won, S. H.; Fenard, Y.; Ju, Y. Uncertainty Assessment of Species Measurements in Acetone Counterflow Diffusion Flames. *Proc. Combust. Inst.* **2013**, *34*, 813–820. https://doi.org/10.1016/j.proci.2012.05.055.
(34) Figura, L.; Carbone, F.; Gomez, A. Challenges and Artifacts of Probing High-Pressure Counterflow Laminar Diffusion Flames. *Proc. Combust. Inst.* **2015**, *35*, 1871–1878. https://doi.org/10.1016/j.proci.2014.05.028.

(35) Gueniche, H. A.; Glaude, P. A.; Dayma, G.; Fournet, R.; Battin-Leclerc, F. Rich Methane Premixed Laminar Flames Doped with Light Unsaturated Hydrocarbons. I. Allene and Propyne. *Combust. Flame* **2006**, *146* (4), 620–634. https://doi.org/10.1016/j.combustflame.2006.07.004.

(36) Liu, D.; Togbé, C.; Tran, L.-S.; Felsmann, D.; Oßwald, P.; Nau, P.; Koppmann, J.; Lackner, A.; Glaude, P.-A.; Sirjean, B.; Fournet, R.; Battin-Leclerc, F.; Kohse-Höinghaus, K. Combustion Chemistry and Flame Structure of Furan Group Biofuels Using Molecular-Beam Mass Spectrometry and Gas Chromatography – Part I: Furan. *Combust. Flame* **2014**, *161*, 748–765. http://dx.doi.org/10.1016/j.combustflame.2013.05.028.

(37) Tran, L.-S.; Glaude, P.-A.; Fournet, R.; Battin-Leclerc, F. Experimental and Modeling Study of Premixed Laminar Flames of Ethanol and Methane. *Energy Fuels* **2013**, *27* (4), 2226–2245. https://doi.org/10.1021/ef301628x.

(38) El Bakali, A.; Boufflers, D.; Betrancourt, C.; Desgroux, P. Experimental and Numerical Investigation of Atmospheric Laminar Premixed N-Butane Flames in Sooting Conditions. *Fuel* **2018**, *211*, 548–565. https://doi.org/10.1016/j.fuel.2017.09.043.

(39) Gasnot, L.; Desgroux, P.; Pauwels, J. F.; Sochet, L. R. Detailed Analysis of Low-Pressure Premixed Flames of $CH_4 + O_2 + N_2$: A Study of Prompt-NO. *Combust. Flame* **1999**, *117*, 291–306. https://doi.org/10.1016/s0010-2180(98)00078-9.

(40) Seiser, R.; Niemann, U.; Seshadri, K. Experimental Study of Combustion of N-Decane and JP-10 in Non-Premixed Flows. *Proc. Combust. Inst.* **2011**, *33* (1), 1045–1052. https://doi.org/10.1016/j.proci.2010.06.078.

(41) Pauwels, J.-F.; Volponi, J. V.; Miller, J. A. The Oxidation of Allene in a Low-Pressure H2/O2/Ar-C3H4 Flame. *Combust. Sci. Technol.* **1995**, *110–111* (1), 249–276. https://doi.org/10.1080/00102209508951926.

(42) Lamoureux, N.; El Merhubi, H.; Pillier, L.; de Persis, S.; Desgroux, P. Modeling of NO Formation in Low Pressure Premixed Flames. *Combust. Flame* **2016**, *163*, 557–575. http://dx.doi.org/10.1016/j.combustflame.2015.11.007.

(43) O'Keefe, A.; Deacon, D. A. G. Cavity Ring-down Optical Spectrometer for Absorption Measurements Using Pulsed Laser Sources. *Rev. Sci. Instrum.* **1988**, *59* (12), 2544–2551. https://doi.org/10.1063/1.1139895.

(44) Evertsen, R.; Van Oijen, J. A.; Hermanns, R. T. E.; De Goey, L. P. H.; Ter Meulen, J. J. Measurements of Absolute Concentrations of CH in a Premixed Atmospheric Flat Flame by Cavity Ring-down Spectroscopy. *Combust. Flame* **2003**, *132* (1), 34–42. https://doi.org/10.1016/S0010-2180(02)00436-4.

(45) Mercier, X.; Desgroux, P. Cavity Ring-Down Spectroscopy for Combustion Studies. In *Cavity Ring-Down Spectroscopy: Techniques and Applications*; Berden, G., Engeln, R., Eds.; Wiley-Blackwell, 2009; p 344.

(46) Evertsen, R.; Staicu, A.; Dam, N.; Van Vliet, A.; Ter Meulen, J. J. Pulsed Cavity Ring-down Spectroscopy of NO and NO2 in the Exhaust of a Diesel Engine. *Appl. Phys. B Lasers Opt.* **2002**, *74*, 465–468. https://doi.org/10.1007/s003400200828.

(47) Lamoureux, N.; Desgroux, P.; El Bakali, A.; Pauwels, J. F. Experimental and Numerical Study of the Role of NCN in Prompt-NO Formation in Low-Pressure $CH_4/O_2/N_2$ and $C_2H_2/O_2/N_2$ Flames. *Combust. Flame* **2010**, *157* (10), 1929–1941. https://doi.org/10.1016/j.combustflame.2010.03.013.

(48) Foo, K. K.; Lamoureux, N.; Cessou, A.; Lacour, C.; Desgroux, P. The Accuracy and Precision of Multi-Line NO-LIF Thermometry in a Wide Range of Pressures and Temperatures. *J. Quant. Spectrosc. Radiat. Transf.* **2020**, *255*, 107257. https://doi.org/10.1016/j.jqsrt.2020.107257.
(49) Foo, K. K.; Lamoureux, N.; Desgroux, P. *Software Thermo NO-LIF*; Université de Lille: pc2a.univ-lille.fr/thermo-no-lif, 2020.
(50) Reisel, J. R.; Carter, C. D.; Laurendeau, N. M. Laser-Induced Fluorescence Measurements of Nitric Oxide in Laminar C2H6/O2/N2 Flames at High Pressure. *Combust. Flame* **1993**, *92*, 485–489. https://doi.org/10.1016/0010-2180(93)90161-u.
(51) Berg, P. A.; Smith, G. P.; Jeffries, J. B.; Crosley, D. R. Nitric Oxide Formation and Reburn in Low-Pressure Methane Flames. *Symp. Int. Combust.* **1998**, *27* (1), 1377–1384. https://doi.org/10.1016/S0082-0784(98)80543-2.
(52) Thomsen, D. D.; Kuligowski, F. F.; Laurendeau, N. M. Background Corrections for Laser-Induced-Fluorescence Measurements of Nitric Oxide in Lean, High-Pressure, Premixed Methane Flames. *Appl. Opt.* **1997**, *36* (15), 3244–3252. https://doi.org/10.1364/AO.36.003244.
(53) Lamoureux, N.; El-Bakali, A.; Gasnot, L.; Pauwels, J. F.; Desgroux, P. Prompt-NO Formation in Methane/Oxygen/Nitrogen Flames Seeded with Oxygenated Volatile Organic Compounds: Methyl Ethyl Ketone or Ethyl Acetate. *Combust. Flame* **2008**, *153* (1–2), 186–201. https://doi.org/10.1016/j.combustflame.2007.07.011.
(54) Istratov, A. A.; Vyvenko, O. F. Exponential Analysis in Physical Phenomena. *Rev. Sci. Instrum.* **1999**, *70*, 1233–1257. https://doi.org/doi:http://dx.doi.org/10.1063/1.1149581.
(55) Piper, L. G.; Cowles, L. M. Einstein Coefficients and Transition Moment Variation for the NO(A 2Σ+–X 2Π) Transition. *J. Chem. Phys.* **1986**, *85* (5), 2419–2422. https://doi.org/10.1063/1.451098.
(56) Zalicki, P.; Zare, R. N. Cavity Ring-down Spectroscopy for Quantitative Absorption Measurements. *J. Chem. Phys.* **1995**, *102* (7), 2708–2717. https://doi.org/10.1063/1.468647.
(57) Mercier, X.; Therssen, E.; Pauwels, J. F.; Desgroux, P. Quantitative Features and Sensitivity of Cavity Ring-down Measurements of Species Concentrations in Flames. *Combust. Flame* **2001**, *124* (4), 656–667. https://doi.org/10.1016/S0010-2180(00)00230-3.
(58) Lamoureux, N.; El Merhubi, H.; Gasnot, L.; Schoemaecker, C.; Desgroux, P. Measurements and Modelling of HCN and CN Species Profiles in Laminar $CH_4/O_2/N_2$ Low Pressure Flames Using LIF/CRDS Techniques. *Proc. Combust. Inst.* **2015**, *35*, 745–752. http://dx.doi.org/10.1016/j.proci.2014.05.126.
(59) Fristrom, R. M. Comments on Quenching Mechanisms in the Microprobe Sampling of Flames. *Combust. Flame* **1983**, *50*, 239–242. https://doi.org/10.1016/0010-2180(83)90065-2.
(60) Kim, Y. C.; Boudart, M. Recombination of O, N, and H Atoms on Silica: Kinetics and Mechanism. *Langmuir* **1991**, *7* (12), 2999–3005. https://doi.org/10.1021/la00060a016.
(61) Guerra, V. Analytical Model of Heterogeneous Atomic Recombination on Silicalike Surfaces. *IEEE Trans. Plasma Sci.* **2007**, *35* (5 I), 1397–1412. https://doi.org/10.1109/TPS.2007.902028.
(62) Cartry, G.; Magne, L.; Cernogora, G. Atomic Oxygen Recombination on Fused Silica: Modelling and Comparison to Low-Temperature Experiments (300 K). *J. Phys. Appl. Phys.* **2000**, *33* (11), 1303–1314. https://doi.org/10.1088/0022-3727/33/11/309.
(63) Mackay, K. K.; Johnson, H. T.; Freund, J. B. Poisoning of Hydrogen Recombination on Silica Due to Water Adsorption. *J. Phys. Chem. C* **2017**, *121* (30), 16366–16372. https://doi.org/10.1021/acs.jpcc.7b04675.

(64) Li, K.; Liu, J.; Liu, W. A New Surface Catalytic Model for Silica-Based Thermal Protection Material for Hypersonic Vehicles. *Chin. J. Aeronaut.* **2015**, *28* (5), 1355–1361. https://doi.org/10.1016/j.cja.2015.08.011.
(65) Gordiets, B.; Ferreira, C. M.; Nahorny, J.; Pagnon, D.; Touzeau, M.; Vialle, M. Surface Kinetics of N and O Atoms in N2-O2 Discharges. *J. Phys. Appl. Phys.* **1996**, *29* (4), 1021–1031. https://doi.org/10.1088/0022-3727/29/4/012.
(66) Glarborg, P.; Miller, J. A.; Ruscic, B.; Klippenstein, S. J. Modeling Nitrogen Chemistry in Combustion. *Prog. Energy Combust. Sci.* **2018**, *67*, 31–68. https://doi.org/10.1016/j.pecs.2018.01.002.
(67) Pauwels, J. F.; Carlier, M.; Devolder, P.; Sochet, L. R. Experimental and Numerical Analysis of a Low Pressure Stoichiometric Methanol-Air Flame. *Combust. Sci. Technol.* **1989**, *64* (1–3), 97–117. https://doi.org/10.1080/00102208908924025.

TOC GRAPHIC

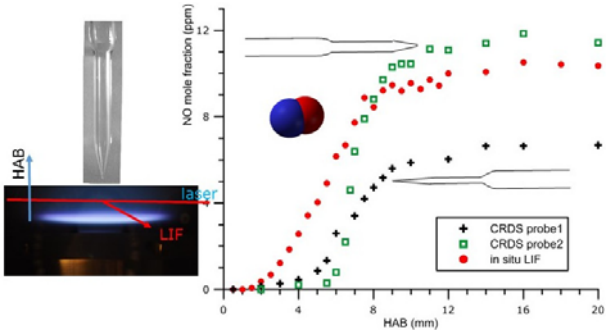
HAB
laser
LIF
NO mole fraction (ppm)
HAB (mm)
CRDS probe1
CRDS probe2
in situ LIF